

Hilbert phase microscopy for investigating fast dynamics in transparent systems

Takahiro Ikeda

Hamamatsu Photonics K. K., 5000 Hirakuchi, Hamakita, Shizuoka 434-8601 Japan

Gabriel Popescu, Ramachandra R. Dasari, and Michael S. Feld

George R. Harrison Spectroscopy Laboratory, Massachusetts Institute of Technology, Cambridge, Massachusetts 02139

Received October 25, 2004

We introduce Hilbert phase microscopy (HPM) as a novel optical technique for measuring high transverse resolution quantitative phase images associated with optically transparent objects. Because of its single-shot nature, HPM is suitable for investigating rapid phenomena that take place in transparent structures such as biological cells. The potential of this technique for studying biological systems is demonstrated with measurements of red blood cells, and its ability to quantify dynamic processes on a millisecond scale is exemplified with measurements of evaporating micrometer-sized water droplets. © 2005 Optical Society of America

OCIS codes: 180.0180, 170.6920, 170.1530.

Optical microscopy has been the most commonly used method of investigation in medicine and biology, and various related technologies have been developed over the past years.¹ Numerous biological samples, including live cells, are quite transparent under visible-light illumination and behave essentially as phase objects. Techniques such as phase contrast and Nomarski microscopy provide contrast of nearly invisible samples by transforming the phase information into the intensity distribution and thus reveal structural details of biological systems.^{2,3} However, the information obtained with these techniques about the phase shift associated with the illuminating field is only qualitative. Retrieving quantitative phase information from transparent objects with high accuracy and low noise allows for novel applications in the biological investigation of structure and dynamics.⁴ Both interferometric⁵ and noninterferometric⁶ techniques have been proposed for quantitative phase imaging of biological samples. Recently Fourier phase microscopy was developed at the MIT Spectroscopy Laboratory as an extremely low-noise phase imaging method.⁷ Because of its subnanometer phase stability over extended periods of time, Fourier phase microscopy is suitable for investigating the dynamics of biological systems on time scales from seconds to a cell lifetime.

However, many processes that take place at the cellular level, including cytoskeletal dynamics,⁸ cell membrane fluctuations,⁹ and neural activity,¹⁰ occur on shorter time scales, down to the millisecond range. Therefore a microscope that permits acquisition of full-field quantitative phase images at kilohertz frame rates may open the door to quantifying unexplored biological phenomena.

Since its introduction by Gabor,¹¹ the complex analytic signal formalism of time-varying fields has found broad applications in optics.¹² In particular, the Hilbert transform relationship between the real and the imaginary parts of a complex analytic signal has been commonly used to retrieve phase shifts from

single temporal interferograms¹³ and for fringe pattern analysis.¹⁴ In this Letter we present a new optical technique for quantitative phase imaging, referred to as Hilbert phase microscopy (HPM), which permits the retrieval of a full-field phase image from a single spatial interferogram recording. This technique extends the concept of analytic continuation to spatially varying fields, in complete analogy with temporal measurements. In HPM, single-shot phase imaging is limited in frame acquisition rate only by the recording device (CCD). This situation contrasts with that of phase shifting, in which multiple recordings are required for retrieving a single phase image.¹⁵ In addition, HPM inherently allows for robust phase unwrapping, which facilitates the study of phase objects much larger than the wavelength of light.

The experimental setup is depicted in Fig. 1. A He–Ne laser is used as a source for an imaging Mach–Zehnder interferometer. In each arm of the interferometer there are two identical telescopic systems with magnification $M=20\times$. The CCD is positioned in the common Fourier plane of the lenses, where an exact (magnified) replica of the sample field is formed. The reference field is slightly tilted with respect to the sample beam to create a uniform fringe structure oriented at 45° with respect to the x and y axes of the CCD. The CCD that we used (C7770, Hamamatsu Photonics) has an acquisition rate of 291 frames/s at the full resolution of 480 × 640 pixels. For a given sample the spatially varying irradiance at the image plane across either the x or the y axis has the form

$$I(x) = I_R + I_S(x) + 2[I_R I_S(x)]^{1/2} \cos[qx + \phi(x)], \quad (1)$$

where I_R and I_S are, respectively, the reference and the sample irradiance distributions, q is the spatial frequency of the fringes, and ϕ is the spatially varying phase associated with the object, i.e., the quantity of interest in our experiments. Equation (1) is analog-

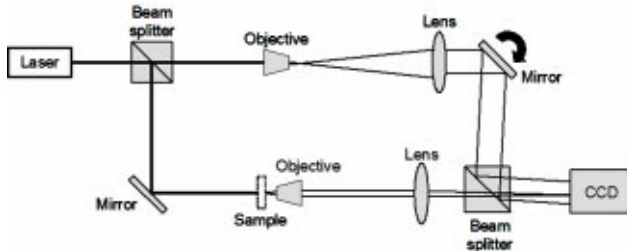


Fig. 1. Experimental setup.

gous to that which describes the temporal interference in Michelson and other interferometers in which q corresponds to the frequency shift introduced by an acousto-optic modulator or a moving mirror. For the transparent objects of interest here, $I_S(x)$ is expected to have a weak dependence on x . By adjusting the magnification of the system, one can choose spatial frequency q to match or exceed the maximum frequency allowed by the numerical aperture of the instrument, such that diffraction-limited resolution is preserved. The sinusoidal term $u(x) = 2\sqrt{I_R I_S} \cos[qx + \phi(x)]$ can thus be isolated by Fourier high-pass filtering. It follows that the complex analytic signal associated with the real function $u(x)$ can be obtained as

$$z(x) = \frac{1}{2}u(x) + i \frac{P}{2\pi} \int_{-\infty}^{\infty} \frac{u(x')}{x - x'} dx'. \quad (2)$$

In Eq. (2) the imaginary part of the right-hand side stands for a principal-value integral, easily identifiable as the Hilbert transform of $u(x)$. Therefore the phase associated with complex analytic signal z is calculated as $\Phi(x) = \tan^{-1}\{\text{Im}[z(x)]/\text{Re}[z(x)]\}$. Note that z exhibits rapid phase modulation with frequency q , and thus Φ is strongly wrapped. However, as q is higher than the spatial-frequency content of the object, the unwrapping procedure works efficiently. Finally, the phase associated with the object is extracted simply as $\phi(x) = \Phi(x) - qx$.

We employed this procedure to retrieve the phase profile of an optical fiber. The fiber core had a diameter of $100 \mu\text{m}$ and a refractive index of 1.457, and the cladding had an outer diameter of $110 \mu\text{m}$ and a refractive index of 1.452. The fiber was immersed in glycerol to better mimic a phase object. The transmission intensity image of this sample [Fig. 2(a)] shows low contrast, which is an indication of the transparency of the sample. Figures 2(b)–2(d) represent intermediate steps in the phase-reconstruction algorithm and correspond to the rectangular area shown in Fig. 2(a). This region encompasses the glycerol-cladding and cladding-core interfaces. The interferogram recorded by the CCD [Fig. 2(b)] is Fourier transformed and high-pass filtered, such that the sinusoidal signal is obtained [Fig. 2(c)]. To obtain the complex analytic signal associated with this real signal we compute the two-dimensional Fourier transform and suppress the negative spatial frequencies. From an inverse Fourier-transform operation a complex two-

dimensional signal is obtained that can provide uniquely the information about the phase of the object, as described in Eq. (2). The strongly wrapped and unwrapped phase images, respectively, are shown in Figs. 2(d) and 2(e). The quantitative phase image of the optical fiber is obtained by subtraction of the linear phase and is depicted in Fig. 2(f), whereas a cross section is shown in Fig. 2(g). The continuous curve in Fig. 2(g) represents the theoretical fit, with the refractive index of glycerol as the variable parameter. The refractive index of glycerol for the best fit had the value $n = 1.467$, which compares well with the values in the literature.

To demonstrate the potential of HPM for biological investigations, we phase-imaged red blood cells from whole blood smears. Figure 2(h) shows an example of such an image, in which the individual cells and the agglomeration of cells are easily identifiable. Red blood cells lack nuclei and major organelles and can be modeled as optically homogeneous objects. Thus the phase information from the HPM images can easily be transformed into thickness information, which provides direct access to parameters such as cell shape and volume. The data were recorded in 10.3 ms, and we prepared the sample by simply sandwiching a droplet of whole blood between two coverslips. The authors are preparing a more-detailed study of the potential of the HPM technique for investigation of the structure and dynamics of blood cells.¹⁶

These results demonstrate the ability of HPM to obtain quantitative phase images in transparent samples. In addition, the technique can measure phase objects with phase profiles much higher than the wavelength of the illuminating light. This impor-

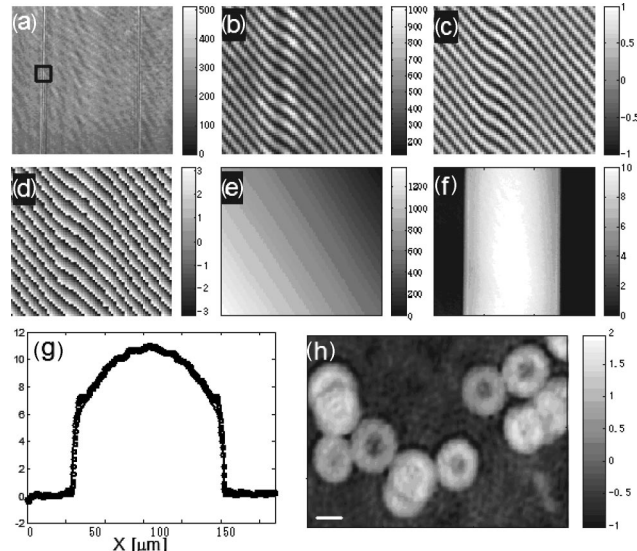


Fig. 2. (a) Transmission intensity image; (b), (c), (d) interferogram, sinusoidal signal, and wrapped phase, respectively, measured from the rectangular area indicated in (a). (e) Full-field unwrapped phase, (f) full-field quantitative phase image, (g) transverse profile through the phase image in *f* with the continuous line indicating the theoretical fit. (h) HPM image of a whole blood smear (magnification, $40\times$) ; a $5\text{-}\mu\text{m}$ scale bar is shown. The gray-scale bars indicate intensity levels for (a)–(c) and the phase in radians for (d)–(h).

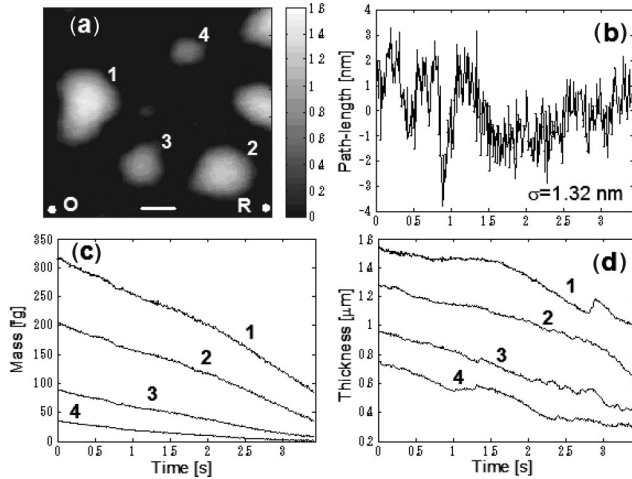


Fig. 3. (a) HPM image of water droplets. The gray-scale bar indicates thickness in micrometers, and the scale bar shows $10 \mu\text{m}$. (b) Path-length fluctuations of point O of (a); the standard deviation is indicated. (c) Temporal evolution of the droplet mass (femtogram units) during evaporation. (d) Maximum thickness of droplets during evaporation. The data were collected over a 3.4-s time interval, with 10.3 ms between successive frames.

tant feature is due to the high spatial modulation imposed on the image, which creates well-defined wrapping points on the phase image, thus facilitating the unwrapping procedure. The ability of HPM to obtain quantitative phase images from single-shot measurements, therefore, permits the monitoring of fast dynamic processes in transparent systems.

A dramatic example of rapid processes in transparent media is the evaporation of micrometer-sized liquid droplets. Figure 3(a) shows the Hilbert phase microscopy image of such water droplets sprayed onto a microscope slide. The z -axis information indicates that the thickness of these droplets is significantly smaller than their transverse size. To monitor this evaporation phenomenon we recorded a series of 333 phase images at time intervals of 10.3 ms. Note that, as each phase image is obtained from one CCD recording, it is not necessary to eliminate noise between the two interferometer arms, a significant advantage over phase-shifting techniques. Thus noise between successive frames does not obscure the phase images, which one can conveniently display by referencing each image to a fixed point in the field of view. This reference point is denoted R in Fig. 3(a). To quantify the residual transversal noise that is present in our phase-image series, we recorded the temporal path-length fluctuations associated with point O in Fig. 3(a). These fluctuations were averaged over an area that corresponded to the diffraction-limited spot of the imaging optics ($0.45 \times 0.45 \mu\text{m}$). The standard deviation of these fluctuations has a value of 1.32 nm , as shown, which indicates that nanometer path-length sensitivity can be obtained on a millisecond time scale. Figure 3(c) shows the evolution of droplet masses during this re-

cording, as calculated from the HPM images. For diffraction-limited transverse resolution and the current phase sensitivity, HPM is sensitive to water evaporation volumes that are remarkably small, of the order of 10^{-18} L . In addition, the quantitative phase images offer detailed three-dimensional information about these homogeneous structures. Thus the temporal dependences of the maximum thicknesses associated with the evaporating droplets can easily be estimated [Fig. 3(d)]. As can be seen, these curves are significantly more irregular (sometimes nonmonotonic) than the time evolution of the mass, which indicates the discontinuous nature of changes in shape during evaporation.

In summary, we have shown that Hilbert phase microscopy can retrieve high transverse resolution quantitative phase images from single-shot measurements with nanometer-level sensitivity. Applying the concept of complex analytic signals to the spatial domain relies on the full analogy that exists between the equations that describe the temporal and spatial fluctuations of electromagnetic fields. HPM should provide a powerful tool for investigating unexplored rapid phenomena in transparent media, including the dynamics of living cells.

This research was carried out at the MIT Laser Biomedical Research Center and was partially supported by National Institutes of Health grant P41 RR 02594 and by Hamamatsu Photonics K. K. G. Popescu's e-mail address is gpopescu@mit.edu.

References

1. D. J. Stephens and V. J. Allan, *Science* **300**, 82 (2003).
2. F. Zernike, *Science* **121**, 345 (1955).
3. F. H. Smith, *Research (London)* **8**, 385 (1955).
4. C. Yang, A. Wax, M. S. Hahn, K. Badizadegan, R. R. Dasari, and M. S. Feld, *Opt. Lett.* **26**, 1271 (2001).
5. G. A. Dunn and D. Zicha, in *Cell Biology: A Laboratory Handbook*, 2nd ed., J. Celis, ed. (Academic, San Diego, 1997), Calif., pp. 44–53.
6. D. Paganin and K. A. Nugent, *Phys. Rev. Lett.* **80**, 2586 (1998).
7. G. Popescu, L. P. Deflores, J. C. Vaughan, K. Badizadegan, H. Iwai, R. R. Dasari, and M. S. Feld, *Opt. Lett.* **29**, 2503 (2004).
8. L. Miao, O. Vanderline, M. Stewart, T. M. Roberts, *Science* **300**, 1405 (2003).
9. A. E. Pelling, S. Sehati, E. B. Gralla, J. S. Valentine, J. K. Gimzewski, *Science* **305**, 1147 (2004).
10. D. A. Dombeck, M. Blanchard-Desce, and W. W. Webb, *J. Neurosci.* **24**, 999 (2004).
11. D. Gabor, *J. Inst. Electr. Eng.* **93**, 329 (1946).
12. M. Born and E. Wolf, *Principles of Optics*, 7th ed. (Cambridge U. Press, Cambridge, 1999), p. 557.
13. G. Popescu and A. Dogariu, *Phys. Rev. Lett.* **88**, 183902 (2002).
14. M. Takeda, H. Ina, and S. Kobayashi, *J. Opt. Soc. Am.* **72**, 156 (1982).
15. K. Creath, *Prog. Opt.* **26**, 349 (1988).
16. G. Popescu, T. Ikeda, K. Badizadegan, R. R. Dasari, and M. S. Feld, are preparing a manuscript to be called “Inverted Hilbert phase microscopy for nanoscale investigation of erythrocyte structure and dynamics.”